Inorganic Chemistry
Article

Inorg. Chem. **2009**, *48*, 6661–6669 **6661**
DOI: 10.1021/ic900593c

Fundamental Differences of Substrate Hydroxylation by High-Valent Iron(IV)-Oxo Models of Cytochrome P450

Laleh Tahsini,[†,‡] Mojtaba Bagherzadeh,[‡] Wonwoo Nam,*[,§] and Sam P. de Visser*[,†]

[†]*The Manchester Interdisciplinary Biocenter and the School of Chemical Engineering and Analytical Science, The University of Manchester, 131 Princess Street, Manchester M1 7DN, United Kingdom,*
[‡]*Chemistry Department, Sharif University of Technology, P.O. Box 11155−3615, Tehran, Iran, and*
[§]*Department of Chemistry and Nano Science, Department of Bioinspired Science, Centre for Biomimetic Systems, Ewha Womans University, Seoul 120−750, Korea*

Received March 27, 2009

An Iron(IV)-oxo heme(+•) complex (Compound I, Cpd I) is the proposed active species of heme enzymes such as the cytochromes P450 and is elusive; therefore, biomimetic studies on active site mimics give valuable insight into the fundamental properties of heme active species. In this work we present density functional theory (DFT) calculations on substrate hydroxylation by a Compound I mimic [Fe^{IV}═O($Por^{+•}$)Cl] and its one-electron reduced form [Fe^{IV}═O(Por)Cl]$^{-}$. Thus, recent experimental studies showed that [Fe^{IV}═O(Por)Cl]$^{-}$ is able to react with substrates via hydride transfer reactions [Jeong, Y. J.; Kang, Y.; Han, A.-R.; Lee, Y.-M.; Kotani, H.; Fukuzumi, S.; Nam, W. *Angew. Chem., Int. Ed.* **2008**, *47*, 7321−7324]. By contrast, theoretical studies on camphor hydroxylation by these two oxidants concluded that the one-electron reduced form of Compound I is a sluggish oxidant of hydroxylation reactions [Altun, A.; Shaik, S.; Thiel, W. *J. Am. Chem. Soc.* **2007**, *129*, 8978−8987]. To resolve the question why the one-electron reduced Compound I is an oxidant in one case and a sluggish oxidant in other cases, we have performed a DFT study on 10-methyl-9,10-dihydro acridine ($AcrH_2$) hydroxylation by [Fe^{IV}═O($Por^{+•}$)Cl] and [Fe^{IV}═O(Por)Cl]$^{-}$. The calculations presented in this work show that both [Fe^{IV}═O($Por^{+•}$)Cl] and [Fe^{IV}═O(Por)Cl]$^{-}$ are plausible oxidants, but [Fe^{IV}═O($Por^{+•}$)Cl] reacts via much lower reaction barriers. Moreover, [Fe^{IV}═O($Por^{+•}$)Cl] reacts via hydride transfer, while [Fe^{IV}═O(Por)Cl]$^{-}$ by hydrogen abstraction. The differences between hydride and hydrogen atom transfer reactions have been rationalized with thermodynamic cycles and shown to be the result of differences in electron abstraction abilities of the two oxidants. Thus, the calculations predict that [Fe^{IV}═O(Por)Cl]$^{-}$ is only able to hydroxylate weak C−H bonds, whereas [Fe^{IV}═O($Por^{+•}$)Cl] is more versatile.

Introduction

High-valent iron(IV)-oxo complexes are common entities in enzymatic systems and have been shown to be active oxidants of heme and nonheme iron monoxygenase and dioxygenase enzymes.[1,2] These iron(IV)-oxo complexes have been isolated and characterized in several enzymes, namely, in the heme enzyme horseradish peroxidase (HRP), as well as in the nonheme iron-enzymes taurine/α-ketoglutarate dioxygenase and α-ketoglutarate dependent halogenase.[3] The cytochromes P450 (P450s) are heme enzymes with importance to human health and involved in key metabolizing reactions in the body by degrading xenobiotics and drugs.[4] Although their active oxidant is elusive, indirect evidence through kinetic isotope effects (KIEs) and product distributions implicates that it is an iron(IV)-oxo heme cation radical species.[5] The iron(IV)-oxo

*To whom correspondence should be addressed. E-mail: sam.devisser@manchester.ac.uk (S.P.dV.), wwnam@ewha.ac.kr (W.N.).

(1) (a) Sono, M.; Roach, M. P.; Coulter, E. D.; Dawson, J. H. *Chem. Rev.* **1996**, *96*, 2841–2888. (b) Groves, J. T. *Proc. Natl. Acad. Sci. U.S.A.* **2003**, *100*, 3569–3574. (c) *Cytochrome P450: Structure, Mechanism and Biochemistry*, 3rd ed.; Ortiz de Montellano, P. R., Ed.; Kluwer Academic/Plenum Publishers: New York, 2004.

(2) (a) Solomon, E. I.; Brunold, T. C.; Davis, M. I.; Kemsley, J. N.; Lee, S.-K.; Lehnert, N.; Neese, F.; Skulan, A. J.; Yang, Y.-S.; Zhou, J. *Chem. Rev.* **2000**, *100*, 235–349. (b) Bugg, T. D. H. *Tetrahedron* **2003**, *59*, 7075–7101. (c) Costas, M.; Mehn, M. P.; Jensen, M. P.; Que, L.Jr. *Chem. Rev.* **2004**, *104*, 939–986.

(3) (a) Chance, B.; Powers, L.; Ching, Y.; Poulos, T. L.; Schonbaum, G. R.; Yamazaki, I.; Paul, K. G. *Arch. Biochem. Biophys.* **1984**, *235*, 596–611. (b) Penner-Hahn, J. E.; Smith Eble, K.; McMurry, T. J.; Renner, M.; Balch, A. L.; Groves, J. T.; Dawson, J. H.; Hodgson, K. O. *J. Am. Chem. Soc.* **1986**, *108*, 7819–7825. (c) Riggs-Gelasco, P. J.; Price, J. C.; Guyer, R. B.; Brehm, J. H.; Barr, E. W.; Bollinger, J. M.; Krebs, C. *J. Am. Chem. Soc.* **2004**, *126*, 8108–8109. (d) Galonić, D. P.; Barr, E. W.; Walsh, C. T.; Bollinger, J. M.; Krebs, C. *Nat. Chem. Biol.* **2007**, *3*, 113–116.

(4) (a) Guengerich, F. P. *Chem. Res. Toxicol.* **2001**, *14*, 611–650. (b) Munro, A. W.; Girvan, H. M.; McLean, K. J. *Nat. Prod. Rep.* **2007**, *24*, 585–609.

(5) (a) Egawa, T.; Shimada, H.; Ishimura, Y. *Biochem. Biophys. Res. Commun.* **1994**, *201*, 1464–1469. (b) Kellner, D. G.; Hung, S. C.; Weiss, K. E.; Sligar, S. G. *J. Biol. Chem.* **2002**, *277*, 9641–9644.

Published on Web 05/26/2009

heme(+•) complex, designated Compound I (Cpd I),[6] is a versatile oxidant that transfers its oxygen atom to substrates to give hydroxylated, epoxidized, or sulfoxidized products.[1] Although Cpd I has escaped experimental detection so far, its precursor in the catalytic cycle, the ferric-hydroperoxo species or Compound 0 (Cpd 0), has been characterized by EPR/ENDOR and resonance Raman spectroscopic studies.[7]

In other heme enzymes, such as peroxidases, either a one-electron reduction or a hydrogen abstraction by Cpd I gives the active oxidant, which is designated Compound II (Cpd II).[8] However, it is generally believed that the hydrogen atom abstraction ability of Cpd II is much weaker than that of Cpd I.[9] Indeed, a recent quantum mechanics/molecular mechanics (QM/MM) study on the relative activities of Cpd I and its one-electron reduced form in a $P450_{cam}$ model predicted sluggish oxidative properties for reduced Cpd I with substrate hydroxylation barriers that are well higher than those observed for Cpd I.[10] More recent experimental studies of Nam, Fukuzumi, and co-workers,[11] by contrast, showed that biomimetic iron(IV)-oxo porphyrin oxidants, that is, Cpd II-mimics, are able to react with substrates via hydrogen abstraction and hydride transfer reactions. Thus, conflicting results in the literature on the hydrogen abstraction abilities of Fe^{IV}-oxo heme(+•) versus Fe^{IV}-oxo heme oxidants warrant further studies to find out which of these two oxidants is more active and what the fundamental factors are that influence this. Therefore, to gain insight into the mechanisms of hydride transfer to either $[Fe^{IV}{=}O(Por^{+\bullet})Cl]$ or $[Fe^{IV}{=}O(Por)Cl]^-$ and the fundamental factors that distinguish it from a hydrogen atom abstraction, we have studied the reaction of $[Fe^{IV}{=}O(Por^{+\bullet})Cl]$ and $[Fe^{IV}{=}O(Por)Cl]^-$ with one of the substrates used in the studies of Fukuzumi et al., namely, 10-methyl-9,10-dihydroacridine ($AcrH_2$). These systems are mimics of biological cofactors often found in proteins and enzymes.[12]

Experimental studies failed to unambiguously identify whether the iron(IV)-oxo species reacts with $AcrH_2$ via hydrogen atom abstraction, hydride transfer, or proton coupled electron transfer (PCET), Scheme 1. Thus, one possibility is the reaction of the oxidant with $AcrH_2$ via hydrogen atom abstraction to give a hydroxo-iron(IV/III) complex and an $AcrH^\bullet$ radical rest-group. Alternatively, a hydride transfer from $AcrH_2$ to Cpd I will lead to a hydroxo-iron(III) complexed with a cationic $AcrH^+$ rest-group, or a hydroxo-iron(II) complexed with $AcrH^+$ from the reaction of $[Fe^{IV}{=}O(Por)Cl]^-$ with $AcrH_2$. Furthermore, separation of the electron and proton transfer processes through a proton-coupled-electron-transfer (PCET) might take place, whereby the overall reaction is the sum of the two processes, hence a hydrogen atom abstraction. Extensive experimental studies have been reported to find out whether the reaction proceeds through a concerted hydride transfer or PCET but conclusive evidence is still lacking.[13] Nevertheless, the reaction was shown to proceed via a significant KIE value of 17 indicative of a rate determining hydrogen/proton abstraction.[11] To establish what the factors are that govern the occurrence of these intermediate states, we have done a detailed density functional theory (DFT) study on $[Fe^{IV}{=}O(Por^{+\bullet})Cl]$ and $[Fe^{IV}{=}O(Por)Cl]^-$ hydroxylation of $AcrH_2$. The studies show that although Cpd I is the better oxidant, $[Fe^{IV}{=}O(Por)Cl]^-$ is also capable of hydroxylating $AcrH_2$.

Scheme 1. Possible Proton and Electron Transfer Reactions from $AcrH_2$

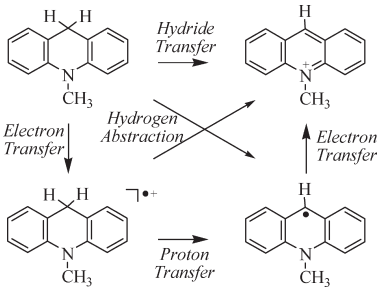

Methods

We use well established and benchmarked procedures and methods[14,15] which we will briefly summarize here. All calculations utilize the hybrid density functional method UB3LYP[16] in combination with a double-ζ quality LACVP basis set on iron and 6-31G on the rest of the atoms, basis set B1.[17] Full geometry optimizations were done in the Jaguar 7.0 program package followed by an analytical frequency calculation.[18] Subsequent single point calculations using a triple-ζ type LACV3P+ basis set on iron and 6-311+G* on the rest of the atoms were done to improve the energetics, basis set B2. In the past we benchmarked these methods against experimental rate constants and kinetic isotope

(6) (a) Denisov, I. G.; Makris, T. M.; Sligar, S. G.; Schlichting, I. *Chem. Rev.* **2005**, *105*, 2253–2277. (b) Meunier, B.; de Visser, S. P.; Shaik, S. *Chem. Rev.* **2004**, *104*, 3947–3980.

(7) (a) Davydov, R.; Makris, T. M.; Kofman, V.; Werst, D. E.; Sligar, S. G.; Hoffman, B. M. *J. Am. Chem. Soc.* **2001**, *123*, 1403–1415. (b) Mak, P. J.; Denisov, I. G.; Victoria, D.; Makris, T. M.; Deng, T.; Sligar, S. G.; Kincaid, J. R. *J. Am. Chem. Soc.* **2007**, *129*, 6382–6383.

(8) (a) Veitch, N. C.; Smith, A. T. *Adv. Inorg. Chem.* **2000**, *51*, 107–162. (b) Paine, M. J. I.; Scrutton, N. S.; Munro, A. W.; Gutierez, A.; Roberts, G. C. K.; Wolf, C. R. Electron Transfer Partners of Cytochrome P450. In *Cytochrome P450: Structure, Mechanism and Biochemistry*; Ortiz de Montellano, P. R., Ed.; Kluwer Academic/Plenum Publishers: New York, 2004; Chapter 4, pp 115−148. (c) Ortiz de Montellano, P. R. *Annu. Rev. Pharmacol. Toxicol.* **1992**, *32*, 89–107.

(9) (a) Nam, W.; Park, S.-E.; Lim, I. K.; Lim, M. H.; Hong, J.; Kim, J. *J. Am. Chem. Soc.* **2003**, *125*, 14674–14675. (b) Nehru, K.; Seo, M. S.; Kim, J.; Nam, W. *Inorg. Chem.* **2007**, *46*, 293–298. (c) Park, M. J.; Lee, J.; Suh, Y.; Kim, J.; Nam, W. *J. Am. Chem. Soc.* **2006**, *128*, 2630–2634.

(10) Altun, A.; Shaik, S.; Thiel, W. *J. Am. Chem. Soc.* **2007**, *129*, 8978–8987.

(11) (a) Jeong, Y. J.; Kang, Y.; Han, A.-R.; Lee, Y.-M.; Kotani, H.; Fukuzumi, S.; Nam, W. *Angew. Chem., Int. Ed.* **2008**, *47*, 7321–7324. (b) Fukuzumi, S.; Kotani, H.; Lee, Y.-M.; Nam, W. *J. Am. Chem. Soc.* **2008**, *130*, 15134–15142.

(12) (a) Stout, D. M.; Meyers, A. I. *Chem. Rev.* **1982**, *82*, 223–243. (b) Gebicki, J.; Marcinek, A.; Zielonka, J. *Acc. Chem. Res.* **2004**, *37*, 379–386. (c) Fukuzumi, S. In *Advances in Electron Transfer Chemistry*; Mariano, P. S., Ed.; JAI press: Greenwich, CT, 1992; pp 67−175.

(13) (a) Pestovsky, O.; Bakac, A.; Espenson, J. H. *J. Am. Chem. Soc.* **1998**, *120*, 13422–13428. (b) Fukuzumi, S.; Ohkubo, K.; Tokuda, Y.; Suenobu, T. *J. Am. Chem. Soc.* **2000**, *122*, 4286–4294.

(14) (a) de Visser, S. P. *J. Am. Chem. Soc.* **2006**, *128*, 9813–9824. (b) de Visser, S. P. *J. Am. Chem. Soc.* **2006**, *128*, 15809–15818. (c) Aluri, S.; de Visser, S. P. *J. Am. Chem. Soc.* **2007**, *129*, 14846–14847. (d) de Visser, S. P.; Tan, L. S. *J. Am. Chem. Soc.* **2008**, *130*, 12961–12974.

(15) (a) de Visser, S. P. *J. Biol. Inorg. Chem.* **2006**, *11*, 168–178. (b) Kim, S. J.; Latifi, R.; Kang, H. Y.; Nam, W.; de Visser, S. P. *Chem. Commun.* **2009**, 1562–1564.

(16) (a) Becke, A. D. *J. Chem. Phys.* **1993**, *98*, 5648–5652. (b) Lee, C.; Yang, W.; Parr, R. G. *Phys. Rev. B* **1988**, *37*, 785–789.

(17) (a) Hay, P. J.; Wadt, W. R. *J. Chem. Phys.* **1985**, *82*, 270–283. (b) Hehre, W. J.; Ditchfield, R.; Pople, J. A. *J. Chem. Phys.* **1972**, *56*, 2257–2261.

(18) *Jaguar 7.0*; Schrödinger, LLC.: New York, 2007.

effects for similar systems and found excellent agreement.[19,20] Thus, in comparison with experimental rate constants, the free energy of activation of styrene epoxidation by cytochrome P450 calculated with B3LYP/B2 was underestimated by 3.1 kcal mol^{-1},[20a] whereas aromatic hydroxylation by a nonheme iron(IV)-oxo oxidant was underestimated by 3.5 kcal mol^{-1}.[20b] Moreover, recent studies on trends in hydrogen abstraction reactions by Cpd I of P450 calculated with these methods and basis sets showed that the barrier heights correlated linearly with the bond dissociation energy of the C−H bond of the substrate with correlation of better than $R^2 = 0.94$.[21] Independent support of this followed from a series of hydrogen abstraction barriers in hydroxylation reactions that were shown to have a mean absolute error below 1 kcal mol^{-1}.[22] Nevertheless, we did a series of test calculations using alternative DFT methods (Supporting Information), which reproduced spin state ordering and relative energies perfectly.

Our model was an iron-oxo group embedded in protoporphyrin IX, whereby all side chains of the heme were abbreviated by hydrogen atoms.[15] The axial ligand was chloride to give a reactant with stoichiometry $FeC_{20}H_{12}N_4OCl$ and overall charge zero (**R1**) or minus one (**R2**). Subsequently, we added 10-methyl-9,10-dihydroacridine ($AcrH_2$), to the chemical system and studied its hydroxylation mechanism. Full optimization of all structures was performed in Jaguar, and an analytical frequency calculation confirmed them as either local minima (with real frequencies only) or transition states (with one imaginary frequency for the correct mode). Since, the experiments of Fukuzumi et al.[11] used a solvent mixture of dichloromethane ($\varepsilon = 8.93$) and acetonitrile ($\varepsilon = 37.5$), we tested the effect of the environment on the reaction energies through single point calculations using the continuum solvent model using a dielectric constant of $\varepsilon = 5.7$ (probe radius 2.72 Å) or $\varepsilon = 33.62$ (probe radius 2.00 Å).

Kinetic isotope effects were estimated from the classical Eyring equations (KIE_E), eq 1, using the difference in free energy of activation ($\Delta G^{\ddagger}$) of the hydrogen and deuterium substituted systems, with R being the gas constant and T the estimated temperature (298.15 K).

$$KIE_E = \exp((-\Delta G_H + \Delta G_D)/RT) \quad (1)$$

Tunneling corrections (Q_t) to the KIE values were added to give the Wigner KIE_W via eq 2 with h being Planck's constant, k the Boltzmann constant, and ν the imaginary frequency in the transition state.

$$KIE_W = KIE_E \times Q_{tH}/Q_{tD} \quad \text{with} \quad Q_t = 1 + (h\nu/kT)^2/24 \quad (2)$$

Results

Recent studies of Fukuzumi, Nam, and co-workers on biomimetic oxygenation reactions of NADH analogues revealed a hydride abstraction mechanism, which contrast the generally observed hydrogen atom abstraction by P450 enzymes.[1,11] Furthermore, it was shown that not only the [Fe^{IV}=O($Por^{+\bullet}$)] (Por = porphyrin) would be able to perform this reaction but also its one-electron reduced form, [Fe^{IV}=O(Por)]. By contrast, QM/MM studies on camphor hydroxylation by these two oxidants predicted sluggish properties of [Fe^{IV}=O(Por)].[10] The only other theoretical study that identified oxidative properties of [Fe^{IV}=O(Por)] is related to the heme-enzyme nitric oxide synthase (NOS),[14c] where DFT modeling showed that Cpd I with a neutral arginine molecule (Cpd I—Arg) in its vicinity will initially react by electron transfer rather than hydrogen abstraction. Thus, to establish the reactivity differences between these two oxidants we set up a model using two representative systems, namely, [Fe^{IV}=O($Por^{+\bullet}$)Cl] and [Fe^{IV}=O(Por)$Cl]^-$, and studied their reactivity pattern versus a common substrate with a weak C−H bond, that is, $AcrH_2$. Earlier calculations of ours showed that an axial chloride ligand behaves similarly as a thiolate ligand as appears in P450 enzymes and as such should be a good model system.[15]

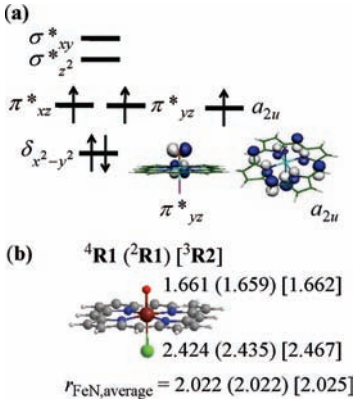

Figure 1. (a) High-lying occupied and low-lying virtual orbitals of ^{4}**R1** with the shapes of the π^*_{yz} and a_{2u} orbitals highlighted. (b) Optimized geometries of ^{4,2}**R1** and ^{3}**R2** with bond lengths in angstroms.

Figure 1 shows the high-lying occupied and low-lying virtual molecular orbitals of [Fe^{IV}=O($Por^{+\bullet}$)Cl] (**R1**) and [Fe^{IV}=O(Por)$Cl]^-$ (**R2**) and their optimized geometries. Thus, both systems are characterized as an Fe^{IV}=O group embedded into a porphyrin ring, which has a cation radical on the heme in **R1** but is closed-shell in **R2**.[23] The high-lying occupied and low-lying virtual orbitals originate from the metal 3d atomic orbitals plus a high-lying nonbonding orbital on the porphyrin ligand that in D_{4h} symmetry has the label a_{2u}.[24] The $\delta_{x^2-y^2}$ orbital is a nonbonding orbital in the plane of the porphyrin, and somewhat higher in energy are two π^* orbitals for the Fe−O interaction (π^*_{xz} and π^*_{yz}) that are singly occupied in **R1** and **R2**. The two σ^* orbitals for the interactions of the metal with the chloride and oxo groups ($\sigma^*_{z^2}$) and with the nitrogen atoms of the porphyrin (σ^*_{xy}) are virtual in the reactants. Thus, Cpd I has orbital occupation $\delta_{x^2-y^2}{}^2\,\pi^*_{xz}{}^1\,\pi^*_{yz}{}^1\,a_{2u}{}^1$, but since the interaction between the π^* and a_{2u} orbitals is small, the system appears in close-lying

(19) (a) Kumar, D.; de Visser, S. P.; Shaik, S. *J. Am. Chem. Soc.* **2003**, *125*, 13024–13025. (b) Kumar, D.; de Visser, S. P.; Sharma, P. K.; Cohen, S.; Shaik, S. *J. Am. Chem. Soc.* **2004**, *126*, 1907–1920. (c) Kumar, D.; de Visser, S. P.; Shaik, S. *J. Am. Chem. Soc.* **2004**, *126*, 5072–5073.

(20) (a) Kumar, D.; de Visser, S. P.; Shaik, S. *Chem.—Eur. J.* **2005**, *11*, 2825–2835. (b) de Visser, S. P.; Oh, K.; Han, A.-R.; Nam, W. *Inorg. Chem.* **2007**, *46*, 4632–4641.

(21) (a) de Visser, S. P.; Kumar, D.; Cohen, S.; Shacham, R.; Shaik, S. *J. Am. Chem. Soc.* **2004**, *126*, 8362–8263. (b) Shaik, S.; Kumar, D.; de Visser, S. P. *J. Am. Chem. Soc.* **2008**, *130*, 10128–10140.

(22) Olsen, L.; Rydberg, P.; Rod, T. H.; Ryde, U. *J. Med. Chem.* **2006**, *49*, 6489–6499.

(23) (a) Green, M. T. *J. Am. Chem. Soc.* **1999**, *121*, 7939–7940. (b) Schöneboom, J. C.; Lin, H.; Reuter, N.; Thiel, W.; Cohen, S.; Ogliaro, F.; Shaik, S. *J. Am. Chem. Soc.* **2002**, *124*, 8142–8151. (c) Schöneboom, J. C.; Neese, F.; Thiel, W. *J. Am. Chem. Soc.* **2005**, *127*, 5840–5853. (d) Bathelt, C. M.; Zurek, J.; Mulholland, A. J.; Harvey, J. N. *J. Am. Chem. Soc.* **2005**, *127*, 12900–12908.

(24) (a) Ghosh, A. *Acc. Chem. Res.* **1998**, *31*, 189–198. (b) Green, M. T. *J. Am. Chem. Soc.* **2000**, *122*, 9495–9499. (c) Ghosh, A. *J. Biol. Inorg. Chem.* **2006**, *11*, 712–724.

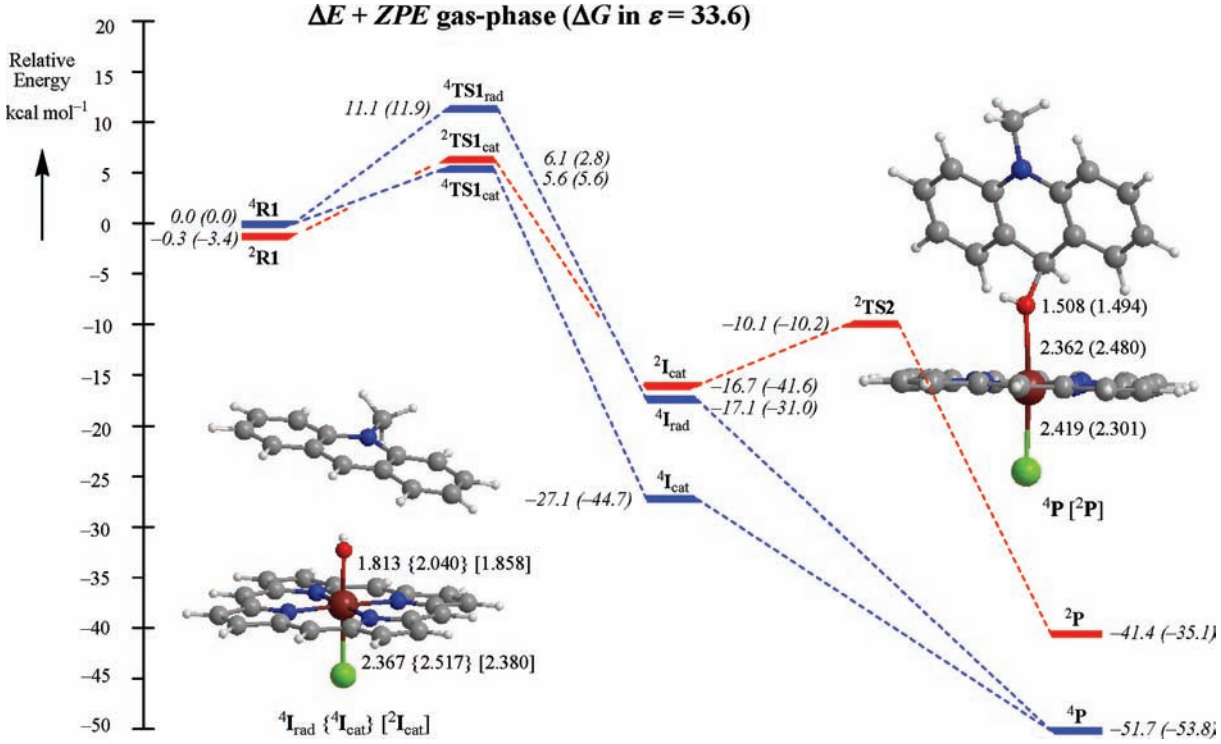

Figure 2. Potential energy profile of $AcrH_2$ hydroxylation by ^{4,2}**R1**. Energies (ΔE + ZPE) and free energies (ΔG) are obtained with Jaguar with energies from basis set B2 while ZPE, entropic, thermal and solvent corrections used basis set B1. Also shown are optimized geometries of intermediate and product complexes with bond lengths in angstroms.

overall quartet and doublet spin states. One electron reduction of quartet and doublet Cpd I fills up the a_{2u} hole with a second electron to give triplet spin **R2** with electronic configuration of $\delta_{x^2-y^2}^2\,\pi^*_{xz}{}^1\,\pi^*_{yz}{}^1\,a_{2u}{}^2$. Since both molecules have an Fe^{IV}-oxo group, the optimized geometries of **R1** and **R2** are very much alike. The only difference is a slightly elongated Fe−Cl bond in **R2** to 2.467 Å. This is the result of the fact that the a_{2u} orbital mixes slightly with a lone pair orbital on the chloride ligand (π_{Cl}) and with double occupation of this orbital there is more antibonding character along the Fe−Cl bond, hence is elongated. These optimized geometries match earlier studies on the same oxidant excellently.[15]

$AcrH_2$ Hydroxylation by [Fe^{IV}=O(Por$^{+\bullet}$)Cl]. First we studied the hydroxylation mechanism of $AcrH_2$ by ^{4,2}**R1** and the obtained potential energy surface is shown in Figure 2. As follows, the reaction is stepwise starting from a long-range reactant complex between **R1** and $AcrH_2$. The initial step is a hydrogen atom or hydride abstraction via barrier ^{4,2}**TS1** leading to either a radical or cationic intermediate (^{4}**I**$_{rad}$, ^{4,2}**I**$_{cat}$). A subsequent OH rebound mechanism via a rebound barrier **TS2** gives hydroxylated product complexes (^{4,2}**P**). In the high-spin state, these rebound barriers are small and negligible (see Supporting Information), but in the low-spin a barrier of about 6.6 kcal mol^{-1} in the gas-phase is encountered.

As expected, the reactant complexes are close in energy and as a consequence give rise to two-state-reactivity patterns (TSR) on competing doublet and quartet spin state surfaces. This is similar to previous DFT studies on the reactivity of heme iron(IV)-oxo complexes with substrates.[21,25] The lowest lying barriers (via ^{4}**TS1**$_{cat}$ and ^{2}**TS1**$_{cat}$), however, are hydride transfer barriers leading to a cationic intermediate (^{4}**I**$_{cat}$ and ^{2}**I**$_{cat}$). These are the first reported hydride transfer barriers of iron(IV)-oxo oxidants, moreover, energetically they are well lower in energy than typical hydrogen abstraction barriers. As a matter of fact of the series of eleven hydrogen abstraction barriers by [Fe^{IV}=O(Por$^{+\bullet}$)SH] reported, only the one for *N*,*N*-dimethyl aniline is of similar magnitude, all others are well higher in energy.[21b]

To make sure that the barriers (^{4,2}**TS1**$_{cat}$) and intermediates (^{4,2}**I**$_{cat}$) are indeed the lowest energy electromers, we attempted to swap molecular orbitals to create radical intermediates. In the high-spin state, we thus located ^{4}**I**$_{rad}$ and ^{4}**TS1**$_{rad}$, both with electronic configuration $\delta_{x^2-y^2}^2\,\pi^*_{xz}{}^1\,\pi^*_{yz}{}^1\,a_{2u}{}^2\,\phi_{Sub}{}^1$ or Fe^{IV}(OH)(Por)Cl–AcrH$^\bullet$. However, the hydrogen abstraction barrier ^{4}**TS1**$_{rad}$ is significantly higher in energy than the hydride transfer barrier (^{4}**TS1**$_{cat}$) and in a similar vein ^{4}**I**$_{rad}$ is at least 10 kcal mol^{-1} higher in energy than ^{4}**I**$_{cat}$ in the gas-phase, which grows to 13.7 kcal mol^{-1} in a dielectric constant of ε = 33.6. Consequently, hydrogen abstraction is an unfavorable process for $AcrH_2$ in favor of an overall hydride transfer reaction.

Optimized geometries show features typical of a hydroxylation reaction; in the intermediates the Fe−O bond is weakened from formally a double bond in **R1** to a single bond. In ^{2}**I**$_{cat}$ and ^{4}**I**$_{cat}$ the metal is in oxidation state Fe^{III} and the orbital occupation is $\delta_{x^2-y^2}^2\,\pi^*_{xz}{}^2\,\pi^*_{yz}{}^1\,a_{2u}{}^2$ in the doublet spin state and $\delta_{x^2-y^2}^2\,\pi^*_{xz}{}^1\,\pi^*_{yz}{}^1\,\sigma^*_{z^2}{}^1$ in the quartet spin state. The extra electron in $\sigma^*_{z^2}$ in the high-spin state adds antibonding character to the Fe−Cl bond that is elongated to 2.517 Å. This has been shown before to be responsible for lengthening the Fe−O and Fe−Cl

(25) Shaik, S.; de Visser, S. P.; Ogliaro, F.; Schwarz, H.; Schröder, D. *Curr. Opin. Chem. Biol.* **2002**, *6*, 556–567.

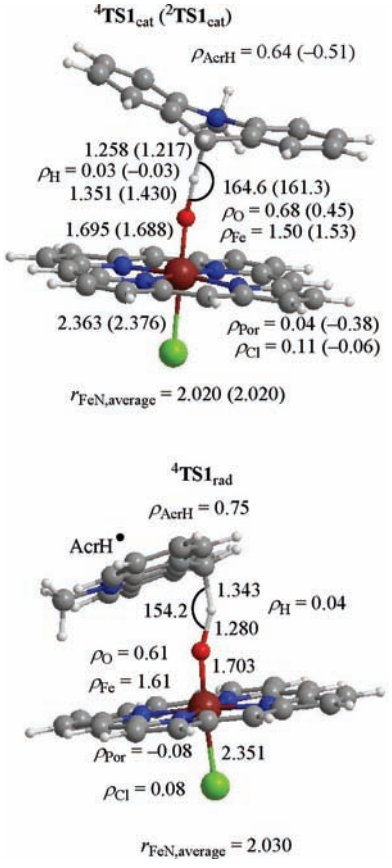

Figure 3. UB3LYP/B1 optimized geometries of ^{4,2}**TS1**$_{cat}$ and ^{4}**TS1**$_{rad}$ as obtained with Jaguar with bond lengths in angstroms. Also given are the group spin densities obtained with basis set B2.

distances, for example, in aromatic hydroxylation reactions.[26] In the product complexes the Fe−O bond is further weakened and will enable release of products.

Optimized geometries and group spin densities of the rate determining transition states (^{4,2}**TS1**$_{cat}$ and ^{4}**TS1**$_{rad}$) are depicted in Figure 3. Geometrically there are no dramatic differences between the three structures: the hydrogen atom is almost midway in between the oxo and carbon atoms, although in the cationic complexes it is somewhat closer on the reactant side. The group spin densities of the structures reveal a ρ_{FeO} of about two in all three structures and significant spin density on the substrate. The spin density on the substrate in ^{4,2}**TS1**$_{cat}$ is lower than that for ^{4}**TS1**$_{rad}$ but is still well larger than that expected for a cationic transition state. Instead, there is significant radical character on the substrate (ρ_{AcrH} = 0.64 in ^{4}**TS1**$_{cat}$ and ρ_{AcrH} = −0.51 in ^{2}**TS1**$_{cat}$). Detailed geometry scans, however, showed ^{4,2}**TS1**$_{cat}$ to relax to the cationic intermediates.

Therefore, although the reaction leading to ^{4,2}**I**$_{cat}$ is formally a hydride transfer reaction, in fact the reaction is a hydrogen atom abstraction coupled electron transfer with the second electron transfer separated from the hydrogen atom transfer. Thus, the hydrogen atom abstraction occurs first; hence, all transition states have similar geometries, electron distributions, and spin densities. The second electron transfer takes place during the pathway from ^{4,2}**TS1**$_{cat}$ to ^{4,2}**I**$_{cat}$. This mechanism is similar to that calculated for *trans*-2-phenyl-isopropylcyclopropane hydroxylation by a P450 model complex where an initial hydrogen atom abstraction barrier precedes a spin crossing from a radical to a cationic potential energy surface and thereby relaxes to a hydride transfer intermediate.[19c]

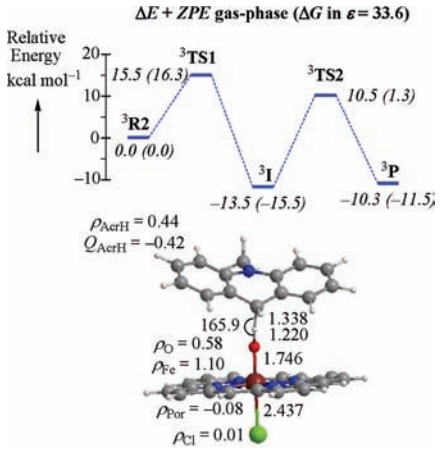

Figure 4. Potential energy profile of $AcrH_2$ hydroxylation by ^{3}**R2**. Relative energies (ΔE + ZPE) and free energies (ΔG) are obtained with Jaguar with energies from basis set B2 while ZPE, entropic, thermal, and solvent corrections with basis set B1. Also shown is the optimized geometry of ^{3}**TS1** with bond lengths in angstroms, the charge on the substrate (Q_{AcrH}), and group spin densities obtained with basis set B2.

$AcrH_2$ Hydroxylation by [Fe^{IV}=O(Por)Cl]$^-$. Subsequently, we studied the hydroxylation of $AcrH_2$ by the one-electron reduced version of **R1**, namely, [Fe^{IV}=O(Por)Cl]$^-$ or **R2**, and the mechanism obtained at the triplet spin state surface is shown in Figure 4. The reaction starts from a long-range complex of [Fe^{IV}=O(Por)Cl]$^-$ with $AcrH_2$ (^{3}**R2**) that similarly to the mechanism shown above for **R1**, reacts in a stepwise mechanism to hydroxylated products. The overall reaction is exothermic by 10.3 kcal mol^{-1} in the gas-phase and 11.5 kcal mol^{-1} in a dielectric constant of ε = 33.6. These exothermicities are much less than those obtained for Cpd I.

The initial reaction is a hydrogen atom abstraction to form a radical intermediate, ^{3}**I**, via a hydrogen abstraction transition state ^{3}**TS1**. Radical rebound via a transition state ^{3}**TS2** gives hydroxylated products (^{3}**P**). A hydrogen abstraction barrier of 15.5 kcal mol^{-1} is found in the gas-phase, which is well higher in energy than the hydride transfer barrier by **R1** of 5.6 kcal mol^{-1}. On the other hand, a hydrogen abstraction barrier by **R1** of 11.1 kcal mol^{-1} leads to a radical intermediate. The hydrogen atom abstraction mechanism by **R2**, therefore, is only 4.4 kcal mol^{-1} higher in energy in the gas-phase than the analogous barrier for **R1** and the only reason **R1** is a more efficient oxidant here is because there is a lower lying hydride transfer mechanism. Consequently, our studies show that although Cpd I is the better oxidant of the two, the difference in hydrogen abstraction barriers is actually quite small. Thus, **R2** should be able to perform hydroxylation reactions although not as efficiently as **R1**. Note that the radical rebound barrier via ^{3}**TS2** is very large (18.4 kcal mol^{-1} in the gas-phase), which means that the radical intermediate is expected to have a finite

(26) (a) de Visser, S. P.; Shaik, S. *J. Am. Chem. Soc.* **2003**, *125*, 7413–7424. (b) de Visser, S. P. *Chem.—Eur. J.* **2006**, *12*, 8168–8177. (c) de Visser, S. P.; Tahsini, L.; Nam, W. *Chem.—Eur. J.* **2009**, *15*, 5577–5587.

Table 1. Kinetic Isotope Effects (KIE) as Calculated with the Eyring (KIE_E) and Wigner (KIE_W) Models for $AcrH_2$ Hydroxylation by ^{4,2}**R1** and ^{3}**R2**[a]

	^{4}**R1**		^{2}**R1**		^{3}**R2**	
	KIE_E	KIE_W	KIE_E	KIE_W	KIE_E	KIE_W
$AcrH_2$/AcrDH	6.11	10.09	4.87	7.15	6.96	11.96
$AcrH_2$/AcrHD	0.94	0.97	1.03	1.12	0.96	0.97
$AcrH_2$/$AcrD_2$	5.84	9.89	5.09	8.05	6.79	11.79

[a] AcrDH has the transferring hydrogen atom replaced by deuterium, and AcrHD, the non-transferring hydrogen atom (i.e., secondary KIE).

lifetime. In previous studies it was shown that large rebound barriers can give rise to byproducts due to rearrangement.[19,27] In this particular case, however, the barrier via ^{3}**TS2** is actually larger than that for ^{3}**TS1**, although by a small amount which implies that rebound rather than hydrogen abstraction will be rate limiting in the reaction mechanism by **R2**.

The hydrogen abstraction barrier ^{3}**TS1** resembles ^{4}**TS1**$_{rad}$ closely; the hydrogen atom is placed midway in between the oxo and carbon atoms, but closer to the oxo group, that is, product-like. The group spin densities show that some spin density has transferred from the oxo group to the substrate, while the spin on the metal remains the same. A small amount of spin density has accumulated on the substrate in ^{3}**TS1**, which grows to a full radical in ^{3}**I**.

To find out whether a hydride transfer reaction would give a different KIE compared to a hydrogen abstraction barrier and additionally discover the KIE differences between **R1** and **R2**, we calculated the free energy of activation of the hydrogen and deuterium substituted barriers. Table 1 displays the KIEs for the hydride transfer mechanisms via ^{4,2}**TS1**$_{cat}$ originating from ^{4,2}**R1** and the radical mechanism from ^{3}**R2** via ^{3}**TS1**. We calculated the effect of replacing the transferring hydrogen atom by deuterium (AcrDH) as well as that for substituting the other hydrogen atom from this CH_2 group by deuterium (in AcrHD), and finally both hydrogen atoms of the CH_2 group were changed to deuterium atoms (in $AcrD_2$). As follows from Table 1, the hydride transfer barriers (from ^{4,2}**R1**) give slightly lower KIE values than the hydrogen atom abstraction barrier via ^{3}**TS1**. The secondary KIE is small and a minor inverse KIE effect is obtained for both ^{4}**R1** and ^{3}**R2**. For the hydrogen abstraction reaction of *trans*-methylphenylcyclopropane by Cpd I of P450 KIE values of around 6−7 for KIE_E and around 8 for KIE_W were calculated.[19] Therefore, our KIE values for ^{3}**R2** are in good agreement with previous calculated values of *trans*-methylphenylcyclopropane hydroxylation by Cpd I of P450.

The imaginary frequencies in the transition states are *i*1340.2, *i*1006.2, and *i*1797.3 cm^{-1} for ^{4}**TS1**$_{cat}$, ^{2}**TS1**$_{cat}$, and ^{3}**TS1**, respectively. Clearly, larger imaginary frequencies represent sharper and narrower reaction barriers and consequently more tunneling may be expected. These imaginary frequencies therefore explain the trends in KIE values reported in Table 1 and explain the slightly higher KIEs for hydrogen atom abstraction by **R2** as compared to hydride transfer by **R1**. The large imaginary frequency for the **R2** pathway gives rise to a relatively large tunneling contribution and hence a significantly higher KIE_W value as compared to the mechanisms from **R1** is observed, see Table 1. Experimentally, a KIE value of 17 for $AcrH_2$/AcrDH hydroxylation by [Fe^{IV}=O(Por)] biomimetic system was observed,[11] which compares reasonably well with the tunneling corrected value of KIE_W = 12 shown in Table 1. The experimental oxidant, however, was Fe^{IV}=O(tpfpp), with tpfpp = *meso*-tetrakis(pentafluorophenyl)porphyrinato dianion, while here we used an oxidant with a chloride axial ligand, which is missing in the experimental setup. Therefore, to find out whether removal of the axial ligand from the oxidant leads to significant differences in reactivity patterns and KIE effects, we did a further set of calculations for Fe^{IV}=O(Por) with $AcrH_2$ (^{3}**R2′**), that is, **R2** without axial ligand (see Supporting Information). Similarly to the studies shown in Figure 4 above, also the reaction of Fe^{IV}=O(Por) with $AcrH_2$ is stepwise with an initial hydrogen atom abstraction leading to a radical intermediate. The hydrogen abstraction barrier (^{3}**TS1′**) for the reaction of $AcrH_2$ by **R2′** is ΔE + ZPE = 14.2 kcal mol^{-1} in the gas-phase, which is within 1.5 kcal mol^{-1} of the value obtained with a chloride axial ligand using the same methods and basis sets. Moreover, a KIE_E = 7.1 and KIE_W = 11.8 for $AcrH_2$ versus AcrDH hydroxylation by Fe^{IV}=O(Por) is calculated. Therefore, the axial ligand has only a minor effect on the reaction and does not influence reaction barriers or KIE values significantly.

Experimentally, a free energy of activation of 17.0 kcal mol^{-1} was obtained for the reaction of Fe^{IV}=O(tpfpp) with $AcrH_2$.[11] This value compares excellently with the calculated free energy of activation in a dielectric constant of ε = 5.7 for [Fe^{IV}=O(Por)Cl] of $\Delta G^{\ddagger}$ = 18.3 kcal mol^{-1} and for [Fe^{IV}=O(Por)] of 16.6 kcal mol^{-1}. The calculations, therefore, reproduce experimental findings excellently and are good mimics of the experimentally studied system.

Discussion

In this work a comparative DFT study on $AcrH_2$ hydroxylation by [Fe^{IV}=O($Por^{+\bullet}$)Cl] and its one-electron reduced form are reported. As follows from Figures 2 and 4 above, both oxidants (**R1** and **R2**) are able to hydroxylate $AcrH_2$ albeit **R1** is a much more efficient oxidant that gives products with much larger reaction exothermicity and with lower rate determining barriers. **R2** reacts with $AcrH_2$ by hydrogen atom abstraction via a rate determining barrier of 15.5 kcal mol^{-1}, which is a value of the same order of magnitude as camphor hydroxylation by a P450 model.[10,21b] However, the oxidative power of **R2** is substantially lower than that observed by **R1**: The rate determining barriers observed for $AcrH_2$ hydroxylation by **R1** of 5.6 (6.1) kcal mol^{-1} via ^{4}**TS1**$_{cat}$ (^{2}**TS1**$_{cat}$) are among the lowest barriers calculated so far for C−H hydroxylation reactions. As a matter of fact only for *N*,*N*-dimethyl aniline similar barriers were obtained, while all other substrates including the natural substrate camphor of $P450_{cam}$ give much higher reaction barriers.[21] So what are the reasons that **R1** is a better oxidant than **R2** and why does **R1** react via an overall hydride abstraction and **R2** via hydrogen atom abstraction? A second

(27) de Visser, S. P.; Ogliaro, F.; Shaik, S. *Angew. Chem., Int. Ed.* **2001**, *40*, 2871–2874.

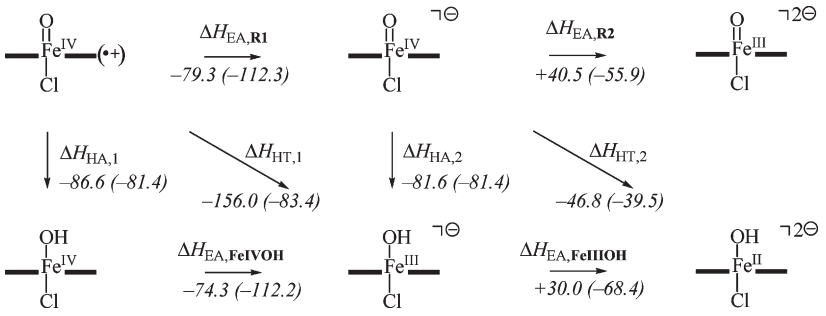

Figure 5. Electron, hydrogen atom (HA), and hydride (HT) transfer energies to bare [Fe^{IV}=O($Por^{+\bullet}$)Cl] and successive intermediates. All energies are in kcal mol^{-1} and obtained at the UB3LYP/B2 level of theory with ZPE at UB3LYP/B1. Values out of parentheses in the gas-phase and inside parentheses with solvent correction included. Reaction energies are defined in eq 3 and 4.

question we will address is what the origin of hydride transfer barriers is. And if they are energetically favorable, why do other reactions take place via hydrogen atom abstraction instead?

Why Is [Fe^{IV}=O($Por^{+\bullet}$)Cl] More Reactive than [Fe^{IV}=O(Por)Cl]$^-$? In the case of the reaction between **R1** and $AcrH_2$ we calculated a mechanism starting with a hydride transfer reaction (via ^{4,2}**TS1**$_{cat}$), as well as one with an initial hydrogen atom abstraction (via ^{4}**TS1**$_{rad}$). The hydride transfer barrier is about 5.5 kcal mol^{-1} lower in energy than the hydrogen atom abstraction. The two hydrogen atom abstraction barriers (via ^{4}**TS1**$_{rad}$ and ^{3}**TS1**) are only 4.4 kcal mol^{-1} different in energy in favor of ^{4}**TS1**$_{rad}$. Notably, using QM/MM methods Thiel et al. found an energy difference of 4.8 kcal mol^{-1} between the barriers for camphor hydroxylation by Cpd I and its one-electron reduced form.[10] This value matches our barrier height difference excellently, and therefore, the protein environment as in P450 enzymes clearly does not influence the relative barriers of substrate hydroxylation by **R1** and **R2**. So what are the fundamental factors that distinguish the hydrogen abstraction barriers of **R1** and **R2** and why does **R1** have a possible alternative via hydride transfer? To answer these questions, we did some further studies on the individual electron, hydrogen atom, and hydride transfer energies of isolated [Fe^{IV}=O($Por^{+\bullet}$)Cl] and [Fe^{IV}=O(Por)Cl]$^-$, and the results are schematically depicted in Figure 5.

Since the structures shown in Figure 5 have different overall charge, we calculated the reaction energies in the gas-phase as well as in a dielectric constant of $\varepsilon = 5.7$. Generally, the gas-phase data give a similar trend to the solvent corrected reactions, but important differences will be highlighted later on. Thus, the energy difference between [Fe^{IV}=O($Por^{+\bullet}$)Cl] and [Fe^{IV}=O(Por)Cl]$^-$ is the electron affinity of Cpd I ($EA_{\mathbf{R1}} = -\Delta H_{EA,\mathbf{R1}}$) and the reduction energy of [Fe^{IV}=O(Por)Cl]$^-$ with another electron is $EA_{\mathbf{R2}}$ (or $-\Delta H_{EA,\mathbf{R2}}$). Reduction of [$Fe^{IV}$=O($Por^{+\bullet}$)Cl] releases 79.3 kcal mol^{-1} in the gas-phase and 112.3 kcal mol^{-1} in a dielectric constant of $\varepsilon = 5.7$. The subsequent electron transfer, by contrast, is endothermic in the gas-phase and has a small exothermicity of 55.9 kcal mol^{-1} in a dielectric constant.

Subsequently we calculated the hydrogen abstraction energy (ΔH_{HA}) as the energy of a complex A to abstract a hydrogen atom to form product AH (eq 3) and the hydride transfer energy (ΔH_{HT}) as the energy of A to abstract a hydride anion to give AH^- (eq 4).

$$A + H\bullet \rightarrow AH\bullet + \Delta H_{HA} \quad (3)$$

$$A + H^- \rightarrow AH^- + \Delta H_{HT} \quad (4)$$

The hydrogen abstraction energy of [Fe^{IV}=O($Por^{+\bullet}$)Cl] to give [Fe^{IV}(OH)(Por)Cl] is 86.6 kcal mol^{-1} in the gas-phase, while that for [Fe^{IV}=O(Por)Cl]$^-$ is only 5.0 kcal mol^{-1} higher in energy. This energy difference is similar to the differences in barrier height between ^{4}**TS1**$_{rad}$ and ^{3}**TS1**. Electronically, hydrogen abstraction by **R1** leads to electron donation into the a_{2u} orbital to give [Fe^{IV}(OH)(Por)Cl] with orbital occupation $\delta^2\,\pi^*_{xz}{}^1\,\pi^*_{yz}{}^1\,a_{2u}{}^2$, whereas hydrogen abstraction by [Fe^{IV}=O(Por)Cl]$^-$ fills the π^*_{xz} orbital with a second electron to give [Fe^{III}(OH)(Por)Cl] with orbital occupation $\delta^2\,\pi^*_{xz}{}^2\,\pi^*_{yz}{}^1\,a_{2u}{}^2$. Since the a_{2u} orbital is slightly below the π^*_{xz} orbital in **R1**, this orbital is filled first with a second electron. The electron transfer to **R2**, as a consequence, is into a higher lying molecular orbital, namely, into one of the π^* orbitals, and as a result the barriers obtained from **R2** are significantly higher than those found for **R1**. However, the energy difference between the a_{2u} and π^* orbitals, in fact, is quite small; hence, the hydrogen abstraction barriers from $AcrH_2$ by **R1** and **R2** differ by only about 4.8 kcal mol^{-1}.

Studies of ethene epoxidation by a Cpd I model of P450 showed a multistate-reactivity pattern via a series of low-lying competitive electronic states.[28] Similarly, a hydrogen abstraction reaction of propene (PH) by Cpd I of P450 or [Fe^{IV}=O($Por^{+\bullet}$)SH] led to five different hydroxo-iron complexes within about 9 kcal mol^{-1}.[29] The reason for this is that simultaneously with the hydrogen atom abstraction one electron is transferred into the iron-heme group. As shown in Figure 1 above the π^*_{xz}, π^*_{yz}, and a_{2u} molecular orbitals are all singly occupied and close in energy. Therefore, electron transfer into the heme, that is, the a_{2u} orbital, gives a hydroxo-iron(IV)-porphyrin complex with electronic configuration $\pi^*_{xz}{}^1\,\pi^*_{yz}{}^1\,a_{2u}{}^2\,\phi_P{}^1$ with either overall doublet or quartet spin, that is, ^{4,2}Fe^{IV}(OH)(Por)SH—P$^\bullet$. Alternatively, an

(28) de Visser, S. P.; Ogliaro, F.; Harris, N.; Shaik, S. *J. Am. Chem. Soc.* **2001**, *123*, 3037–3047.

(29) (a) de Visser, S. P.; Ogliaro, F.; Sharma, P. K.; Shaik, S. *Angew. Chem., Int. Ed.* **2002**, *41*, 1947–1951. (b) de Visser, S. P.; Ogliaro, F.; Sharma, P. K.; Shaik, S. *J. Am. Chem. Soc.* **2002**, *124*, 11809–11826.

electron transfer into one of the π^* orbitals retains the radical on the heme but changes the oxidation state of the metal to Fe(III), that is, $^{4,2}Fe^{III}(OH)(Por^{+\bullet})SH—P^{\bullet}$ with electronic configuration $\pi^*_{xz}{}^2\ \pi^*_{yz}{}^1\ a_{2u}{}^1\ \phi_P{}^1$. There are one quartet spin and two doublet spin configurations with this electron distribution. In the gas-phase the hydroxo-iron complexes with the metal in oxidation state Fe(III) were found to be less stable than the Fe(IV) complexes by about 4.8 kcal mol^{-1}.[29] This energy gap between $Fe^{IV}(OH)(Por)SH—P^{\bullet}$ and $Fe^{III}(OH)(Por^{+\bullet})SH—P^{\bullet}$ is identical to the calculated energy difference between the hydrogen abstraction barriers of $AcrH_2$ by **R1** and **R2** reported here and therefore reflects the energy difference between the π^*_{xz} and a_{2u} molecular orbitals. Thus, **R2** is a lesser oxidant than **R1** because the a_{2u} orbital is already doubly occupied and not accessible for additional electrons, and the lowest lying available orbital is one of the π^* orbitals instead. Because the close degeneracy of the π^* and a_{2u} orbitals, **R2** is still able to act as an oxidant but because a higher lying molecular orbital is filled in the process this will cost substantially more energy than the same process starting from Cpd I. Consequently, the relative oxidative properties of $[Fe^{IV}{=}O(Por^{+\bullet})Cl]$ and its one electron reduced species follow from orbital occupation and the ability of the oxidant to accept electrons.

In addition to the ΔH_{EA} and ΔH_{HA} values in Figure 5, we report the hydride transfer energies (ΔH_{HT}). Thus, hydride transfer to Cpd I gives an $[Fe^{III}(OH)(Por)Cl]^-$ complex, which is the thermodynamic sum of a hydrogen atom transfer followed by electron transfer. As can be seen from Figure 5, the hydride transfer reaction is strongly exothermic for $[Fe^{IV}{=}O(Por^{+\bullet})Cl]$ (by 156.0 kcal mol^{-1} in the gas-phase) but much less exothermic for $[Fe^{IV}{=}O(Por)Cl]^-$. This implies that in the gas-phase, hydride transfer would be the favorable mechanism although it, of course, would be dependent on the relative stability of $Sub^{\bullet}$ versus Sub^+, with Sub the rest-group of the substrate (SubH). The values for ΔH_{HT} are close to the sum of the individual hydrogen abstraction and electron transfer processes, that is, $\Delta H_{HT,1} = \Delta H_{HA,1} + \Delta H_{EA,\mathbf{FeIVOH}} + EA_H$, whereby EA_H represents the electron affinity of a hydrogen atom (EA_H = 4.8 kcal mol^{-1} in the gas-phase). Thus, in the case of $[Fe^{IV}{=}O(Por^{+\bullet})Cl]$, the values for $\Delta H_{HA,1}$ and $\Delta H_{EA,\mathbf{FeIVOH}}$ are very similar, but for the hydride transfer from $[Fe^{IV}{=}O(Por)Cl]^-$ the value $\Delta H_{EA,\mathbf{FeIIIOH}}$ is endothermic. Therefore, the overall reaction of hydride transfer from $[Fe^{IV}{=}O(Por)Cl]^-$ is only slightly exothermic, and hydride transfer cannot compete with hydrogen atom abstraction; hence, hydrogen atom abstraction is the dominant mechanism from $[Fe^{IV}{=}O(Por)Cl]^-$, in agreement with what we found for $AcrH_2$ hydroxylation. In the case of Cpd I, the reaction energies for $\Delta H_{HA,1}$ and $\Delta H_{HT,1}$ in a dielectric constant of $\varepsilon = 5.7$ are close in energy so that the two mechanisms are competitive and the relative stability of $Sub^{\bullet}$ versus Sub^+ determines which of the two mechanisms will be energetically favorable.

Equations 5 and 6 give the overall hydride transfer reaction from Cpd I and the exothermicity ($\Delta H_{eq\ 5}$) described as a function of the bond dissociation energy (BDE_{SubH}) of the substrate, the ionization energy of the substrate rest-group (IE_{Sub}) and EA_H, whereby BDE_{SubH} reflects the energy to split SubH into $Sub^{\bullet}$ and a hydrogen atom, that is, $BDE_{SubH} = -\Delta H_{HA,SubH}$ (eq 3).

$$[Fe^{IV}{=}O(Por^{+\bullet})Cl] + SubH \rightarrow [Fe^{III}(OH)(Por)Cl]^- + Sub^+ \quad (5)$$

$$\Delta H_{Eq5} = \Delta H_{HT,1} - BDE_{SubH} + IE_{Sub} - EA_H \quad (6)$$

Similarly, the overall reaction for the hydrogen atom abstraction by Cpd I is

$$[Fe^{IV}{=}O(Por^{+\bullet})Cl] + SubH \rightarrow [Fe^{IV}(OH)(Por)Cl] + Sub^{\bullet} \quad (7)$$

$$\Delta H_{Eq7} = \Delta H_{HA,1} - BDE_{SubH} \quad (8)$$

Cpd I is most likely to react via hydride transfer if the reaction exothermicity for this reaction is larger than that for hydrogen atom transfer, that is, $\Delta H_{eq\ 5} > \Delta H_{eq\ 7}$, combining this with eqs 6 and 8 gives eq 9.

$$\Delta H_{HT,1} - \Delta H_{HA,1} > EA_H - IE_{Sub} \quad (9)$$

The difference in energy between the hydride transfer and hydrogen atom abstraction energies (Figure 5) is approximately the difference of EA_H and $-\Delta H_{EA,\mathbf{FeIVOH}}$. As a consequence this implies that if IE_{Sub} is smaller than $-\Delta H_{EA,\mathbf{FeIVOH}}$, Cpd I is most likely to react via hydride transfer, whereas in the case $-\Delta H_{EA,\mathbf{FeIVOH}} < IE_{Sub}$ the reaction most likely will proceed via a hydrogen atom abstraction instead. Thus, $-\Delta H_{EA,\mathbf{FeIVOH}}$ is 112.2 kcal mol^{-1} in a dielectric constant of $\varepsilon = 5.7$, whereas IE_{Sub} is calculated to be 92.9 kcal mol^{-1} using the same methods and basis sets. Therefore, the value of $-\Delta H_{EA,\mathbf{FeIVOH}}$ is larger than that of IE_{Sub}; hence, Cpd I reacts via a hydride transfer rather than hydrogen atom abstraction as indeed observed in Figure 2.

In the case of $[Fe^{IV}{=}O(Por)Cl]^-$ the difference between the hydride transfer and hydrogen atom abstraction reaction is determined by the relative energy of $\Delta H_{EA,\mathbf{FeIIIOH}}$ and IE_{Sub}. However, $-\Delta H_{EA,\mathbf{FeIIIOH}}$ is very small (68.4 kcal mol^{-1}), well lower than IE_{Sub} of 92.9 kcal mol^{-1}, so that $[Fe^{IV}{=}O(Por)Cl]^-$ reacts via hydrogen atom abstraction rather than hydride transfer. As a result only few substrates (if at all) will have an ionization potential that is low enough to react with $[Fe^{IV}{=}O(Por)Cl]^-$ by hydride transfer instead. Indeed, our studies presented in this work show that $[Fe^{IV}{=}O(Por)Cl]^-$ reacts via a dominant hydrogen abstraction, whereas $[Fe^{IV}{=}O(Por^{+\bullet})Cl]$ via hydride abstraction. In conclusion, hydride and hydrogen atom transfer reactions are based on the electron affinity of the hydroxo-iron complex and the ionization potential of the Sub rest-group. Since, $\Delta H_{EA,\mathbf{FeIVOH}}$ is highly exothermic and $\Delta H_{EA,\mathbf{FeIIIOH}}$ not, $[Fe^{IV}{=}O(Por^{+\bullet})Cl]$ reacts via hydride transfer while $[Fe^{IV}{=}O(Por)Cl]^-$ is unable to do that. In the past we showed that this reaction exothermicity can be transferred to a reaction barrier.[21]

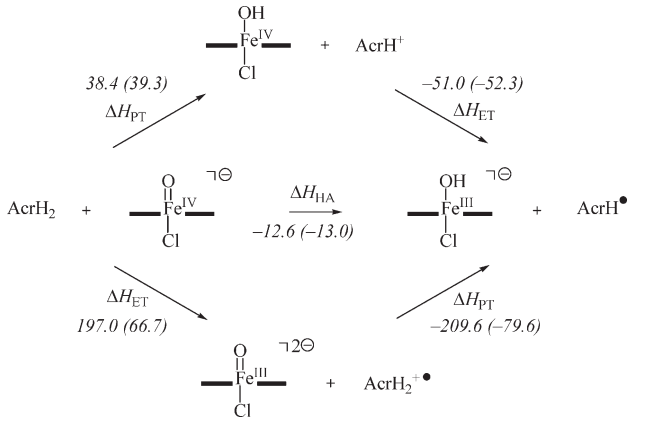

Figure 6. Comparative reaction energies for hydrogen abstraction (middle) of $AcrH_2$ by **R2** and two possible PCET mechanisms. All energies are in kcal mol^{-1} and are obtained with basis set B2 with ZPE corrections at B1 level of theory. Data out of parentheses in the gas-phase and in parentheses calculated in a dielectric constant of $\varepsilon = 5.7$.

Does $[Fe^{IV}{=}O(Por)Cl]^-$ React via Hydrogen Atom Abstraction or Proton Coupled Electron Transfer? In the previous section we showed that $[Fe^{IV}{=}O(Por)Cl]^-$ reacts with $AcrH_2$ via a formal hydrogen abstraction reaction and not via hydride transfer. However, a hydrogen abstraction mechanism is formally the sum of an electron and proton transfer. These two processes not necessarily proceed simultaneously. In particular, separation of electron and proton transfer processes is described as a proton-coupled-electron-transfer (PCET). Figure 6 displays the reaction energies for hydrogen abstraction in the center, which are slightly exothermic in the gas-phase (by −12.6 kcal mol^{-1}). This reaction energy compares excellently with our relative energy between ^{3}**R2** and ^{3}**I** (see above in Figure 4 above) of −13.5 kcal mol^{-1}. Therefore, the interaction between the two reactant and two intermediate structures in complexes ^{3}**R2** and ^{3}**I** have little effect on the reaction energetics.

Subsequently, we calculated the energy of **R2** to abstract an electron from $AcrH_2$ followed by a proton abstraction to give the hydrogen abstraction intermediate (lower mechanism in Figure 6). As follows the initial electron transfer is highly endothermic, although much of the energy is released again in the proton transfer to give an overall slightly exothermic reaction. Nevertheless, the high cost of the initial electron transfer makes this an unlikely mechanism.

The alternative was tested and shown at the top of Figure 6, where the proton transfer precedes the electron transfer. The first step is endothermic by about 38.4 kcal mol^{-1} in the gas-phase and a similar value in a dielectric constant was found. The subsequent electron transfer is exothermic and gives an overall reaction energy of 12.6 kcal mol^{-1}, similar to that obtained for the direct hydrogen abstraction. Nevertheless, the individual reactions shown in Figure 6 clearly show that only a low-energy mechanism is obtained when the electron and proton transfer are coupled together into a hydrogen abstraction mechanism (middle of Figure 6). Therefore, DFT studies show that an alternative PCET mechanism is energetically less favorable over a direct hydrogen atom transfer by $[Fe^{IV}{=}O(Por)Cl]^-$.

Conclusion

DFT calculations on $AcrH_2$ hydroxylation by two iron (IV)-oxo oxidants are reported: $[Fe^{IV}{=}O(Por^{+\bullet})Cl]$ and $[Fe^{IV}{=}O(Por)Cl]^-$. The former, that is, Cpd I, is an efficient oxidant that reacts via hydride abstraction with low reaction barriers of 5.6 kcal mol^{-1}. The hydride transfer, in fact, is an initial hydrogen abstraction followed by a rapid electron transfer leading to a cationic intermediate. Although $[Fe^{IV}{=}O(Por)Cl]^-$ is able to hydroxylate $AcrH_2$, its barriers are significantly higher than those found for Cpd I. This is mainly because the hydride transfer reaction is thermodynamically unfavorable and only a hydrogen abstraction reaction can take place. Comparable hydrogen abstraction reactions by the two oxidants are about 5 kcal mol^{-1} different in energy and as a consequence the difference in barrier heights has the same energy gap. We have set up a valence bond (VB) model to explain the electronic differences between the two reaction mechanisms. Moreover, a thermodynamic model is given that explains why some oxidants react via hydride transfer, while others with the same substrate react via hydrogen atom abstraction instead.

Acknowledgment. The research was supported by CPU time provided by the National Service of Computational Chemistry Software (NSCCS). Financial support from the Korea Science and Engineering Foundation and the Ministry of Science and Technology of Korea through the CRI Program and the WCU project (R31-2008-000-10010-0) is acknowledged. L.T. acknowledges the British Council for a Scholarship.

Supporting Information Available: Cartesian coordinates of all structures described in this work, tables with group spin densities, charges and relative energies, and figures with results of geometry scans. This material is available free of charge via the Internet at http://pubs.acs.org.